http://dx.doi.org/10.5012/bkcs.2012.33.7.2315

Comparative Study and Electrochemical Properties of $LiFePO_4F$ Synthesized by Different Routes

Bin Huang,[†,‡] Suqin Liu,[†,‡,*] Hongliang Li,[†,‡] Shuxin Zhuang,[†,‡] and Dong Fang[†,‡]

[†]*College of Chemistry and Chemical Engineering, Central South University, Changsha 410083, China*
[‡]*Key Laboratory of Resources Chemistry of Nonferrous Metals, Chinese Ministry of Education*
[*]*E-mail: sqliu2003@126.com*
Received February 8, 2012, Accepted April 16, 2012

To improve the performance of $LiFePO_4F$, a novel sol-gel process is developed. For comparison, ceramic process is also implemented. From X-ray diffraction results we know that each sample adopts a triclinic $P\bar{1}$ space group, and they are isostructural with amblygonite and tavorite. The scanning electron microscope images show that the homogeneous grains with the dimension of 300-500 nm is obtained by the sol-gel process; meanwhile the sample particles obtained by ceramic process are as big as 1000-3000 nm. By galvanostatic tests and at electrochemical impedance spectroscopy method, the sample obtained by sol-gel process presents better electrochemical properties than the one obtained by ceramic process.

Key Words : $LiFePO_4F$, Tavorite, Sol-gel preparation

Introduction

For the past few years, the family of alkali-metal transition-metal fluoro(hydroxyl) phosphates/fluorosulfates has interested researchers owing to their three-dimensional (3D) framework which can apply a fast-migration channel system for Li^+ to insertion/extraction. Therefore, this type of materials becomes a candidate of the new-generation cathode material for Li^+ batteries.[1-3] Recently, it was reported that $LiZnSO_4F$ with a 3D structure framework was adequate for a ceramic electrolyte,[4] and the ferrous homologue $LiFeSO_4F$ and $NaFeSO_4F$ were reported as intriguing electrode materials[2,5] with obvious advantages such as low toxicity and high Li^+ diffusivity. The analogues based on PO_4F^{4-} polyanion (*e.g.* $LiFePO_4F$, $LiTiPO_4F$ and $LiVPO_4F$) were also reported to be excellent electrochemical performance.[1,6-9]

For $LiFePO_4F$, one Li^+ can be cycled reversibly with the theoretical capacity of 153 $mAh{\cdot}g^{-1}$. The results, obtained by Ramesh *et al.*, proved that the lithium iron fluorophosphates $LiFePO_4F$ was an adequate material for the prospective applications of Li^+ batteries due to its facile Li^+ migration.[1] In order to synthesize $LiFePO_4F$, ceramic process[1,9] and ionothermal process[9] was reported before. However, the solvents used in the ionothermal process are very expensive ionic liquids. More low-cost and feasible methods for synthesis of this material should be explored.

Recently we have successfully synthesized $LiFePO_4F$ by a novel sol-gel process. This method will produce sub-micron particles of $LiFePO_4F$ with excellent electrochemical properties. In this paper, the sol-gel process followed by heat treatments and a traditional ceramic method guided by Ramesh *et al.*[1] were implemented to obtain $LiFePO_4F$. At the same time, we compared the microstructure and electrochemical performance of the materials obtained by the two methods.

Experimental

Sol-gel Synthesis. Stoichiometric quantities of ferrous sulfate and orthophosphoric acid are dissolved in deionized water to form light green solution. Hydrogen peroxide was dripped in the solution in order to oxide the Fe^{2+} to Fe^{3+} and then the solution changed into yellow suspension. Subsequently oxalic acid was added and the suspension was clear again. The pH value was adjusted to 7 followed by mixing CH_3COOLi and NH_4F. The final suspension contained Li/Fe/P/F in a 1:1:1:1 ratio was dried in an oil bath at 80 °C with magnetic stirring overnight. The obtained yellow-green xerogel was putted in a muffle furnace at 350 °C for 5 hours, followed by calcination at 550 °C in air for 2 hours, and then the final powder (labeled as LFPF-1) was obtained after grinding.

Ceramic Synthesis. Stoichiometric quantities of $FePO_4$ and LiF were mixed and heated at 575 °C for 75 min in an argon flow[1], the obtained powder was labeled as LFPF-2. In our research, $Li_3Fe_2(PO_4)_3$ was obtained in our trial guided by the route proposed by J. Barker *et al.*.[10]

Characterizations. X-ray diffraction (XRD) patterns were measured using a JapanD/max2550 diffractometer (Cu Kα, 1.54178 Å) under a 40 kV potential and 300 mA current. The diffraction data were collected at step mode over the angular range of 10-80 degrees with a step size 0.02 degree. The scanning electron microscope (SEM) images were obtained by a JSM-6360LV scanning electron microscope.

For electrochemistry studies, the as-prepared $LiFePO_4F$ was grinded with acetylene black (Super P) for 20 minutes. Then, the mixture was blended with poly(tetrafluoroethylene) (PTFE) to form a lump of paste followed by pressing onto aluminum foil and dried at 110 °C overnight in a vacuum oven, the weight ratio of the samples, Super P and PTFE was 80:10:10, The loading amount of active material

was about 5 mg·cm^{-2}. Afterwards, the CR2016 coin cell with a metallic lithium anode was assembled in a glove box (M BRAUN) under Ar with O_2 and H_2O lower than 10 ppm. For investigating the charging and discharging performance, cells were cycled between 1.8 V and 4.2 V in the galvanostatic mode using a Land CT2001C cell test system (Wuhan, China) at room temperature. For studying the Li^+ diffusion coefficient, electrochemical impedance spectroscopy (EIS) measurement was conducted by Parstat 2273 electrochemical working station, with a frequency range of 100 mHz to 100 kHz and an excitation amplitude of 5 mV.

Results and Discussion

Structural Characterizations. The XRD pattern for the as-prepared $LiFePO_4F$, shown in Figure 1, indicates that each sample is single phase of $LiFePO_4F$. Each sample adopts triclinic $P\bar{1}$ space group with the lattice parameters listed in Table 1. The results in this paper are similar to that of the tavorite $LiFePO_4(OH)$ (JCPDS:41-1376) obtained by Nicolas Marx *et al.*,[6] which demonstrates the isostructuralism between $LiFePO_4F$ and $LiFePO_4(OH)$. Figure 2 shows the SEM images of the as-prepared powder. Figure 2(a) and Figure 2(c) are the overall view (ten thousand-fold magnification) of LFPF-1 and LFPF-2 respectively. In Figure 2(b), it can be clearly seen that the particle sizes of LFPF-1 are 300-500 nm, meanwhile Figure 2(d) shows that the particle sizes of LFPF-2 are 1000-3000 nm.

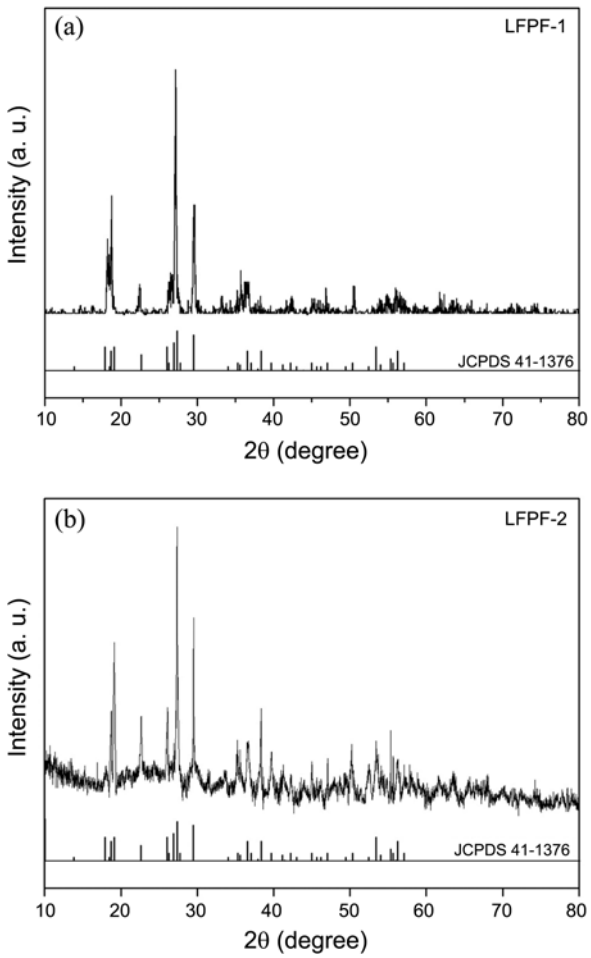

Figure 1. XRD patterns of (a) LFPF-1 and (b) LFPF-2.

Based on the SEM results, we propose a formation mechanism of sub-micron LFPF-1, which is shown in Figure 3. When the xerogel precursor was ready, Li^+, Fe^{2+}, Fe^{3+}, PO_4^{3-}, F^- were uniformly distributed. After 5 hours calcination at 350 °C, the organics were dehydrated completely, only carbon remained and vesicular pores formed. Then the porous precursor was ground, the reactants were restricted in carbon microspheres. After that, the precursor/C composite was calcined at 550 °C for 2 hours, the sub-micron $LiFePO_4F$ formed and the carbon disappeared gradually.

As we known, smaller particle can supply shorter paths for Li^+ diffusion and has larger specific surface area, so in electrodes production, finer active materials powders are preferred. In regard to this, the following electrochemical characterizations would reveal whether the smaller dimension of material particles would benefit for electrochemical performance.

Electrochemical Characterizations. The results of galvanostatic discharge-charge performances at 0.1 C are shown in Figure 4(a). The curve corresponding to LFPF-1 shows a high initial specific capacity of 145 mAh·g^{-1} and a pair of flat plateaus around 2.8 V, indicating a facile Li^+ intercalation for $LiFePO_4F$. This is identical to that of other groups.[1,9] LFPF-2 exhibits a bit lower initial capacity of 136

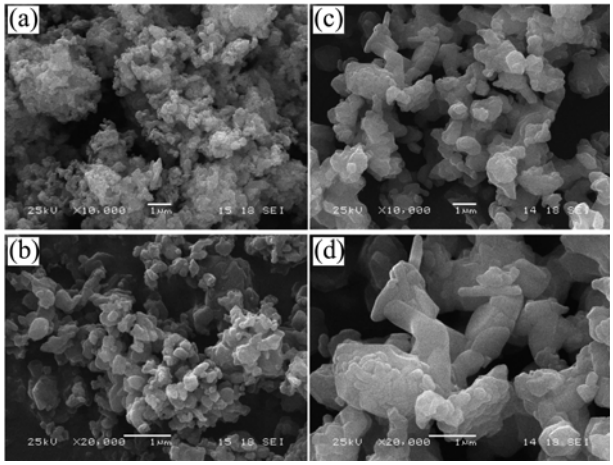

Figure 2. SEM patterns of (a, b) LFPF-1 and (c, d) LFPF-2.

Table 1. Lattice parameters of LFPF-1 and LFPF-2

Sample	*a* (Å)	*b* (Å)	*c* (Å)	α (°)	β (°)	γ (°)	*V* (Å^3)
LFPF-1	5.34023	7.24818	5.07321	108.5199	98.2166	106.7507	172.21
LFPF-2	5.32810	7.26458	5.10301	109.5623	97.6108	106.4285	172.79

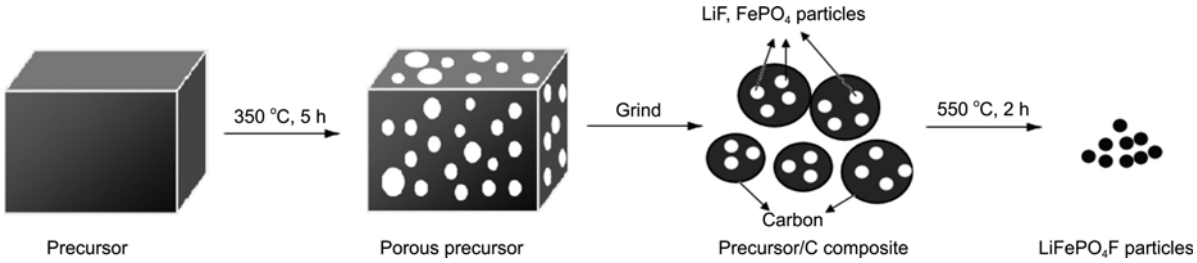

Figure 3. Formation mechanism of LFPF-1.

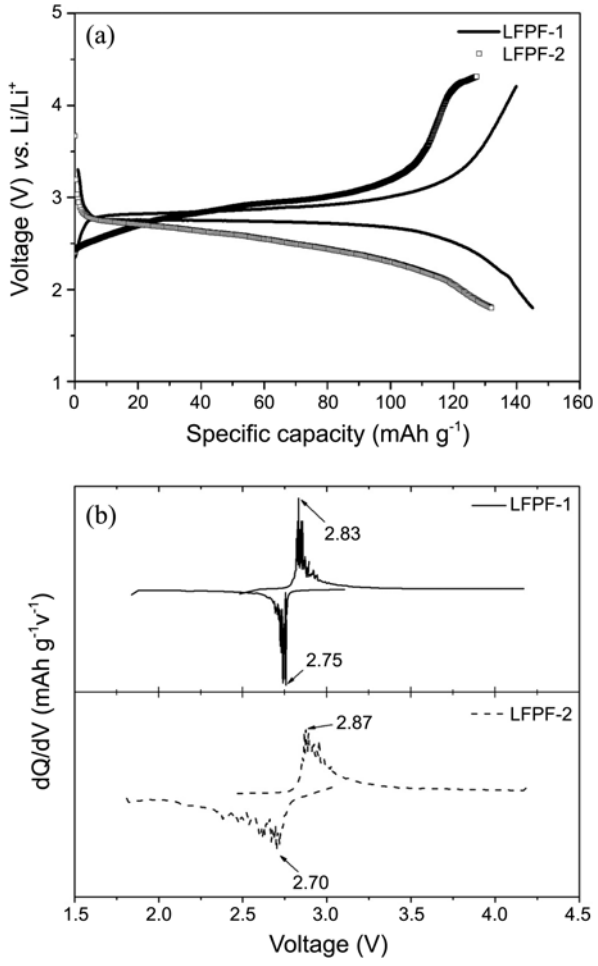

Figure 4. (a) Discharge-charge curves at 0.1 C rate. (b) Differential capacity *vs.* voltage plots derived from the discharge-charge curves.

mAh·g^{-1}. Figure 4(b) is the differential capacity *versus* voltage plot derived from the discharge-charge profile (Fig. 4(a)). For LFPF-1, a couple of peaks show the discharging and charging plateaus at 2.75 V and 2.83 V respectively. The narrow peak separation (0.08 V) indicates that the over potential on Li^+ insertion/extraction is fairly low. In the case of LFPF-2, the potential separation between the two peaks is 0.17 V, indicating a larger polarization occurred. Figure 5 shows the cycle performances (0.1 C) of LFPF-1 and LFPF-2. It can be seen that the specific capacity of LFPF-1 is higher than that of LFPF-2. Therefore, the electrochemical performances were enhanced by the sol-gel method. After

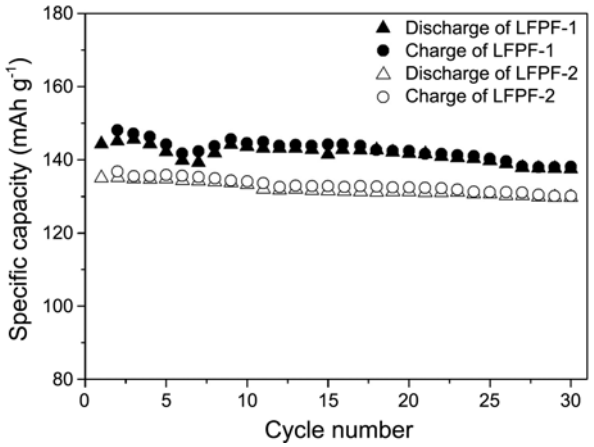

Figure 5. Cyclic performances of the two samples at 0.1 C.

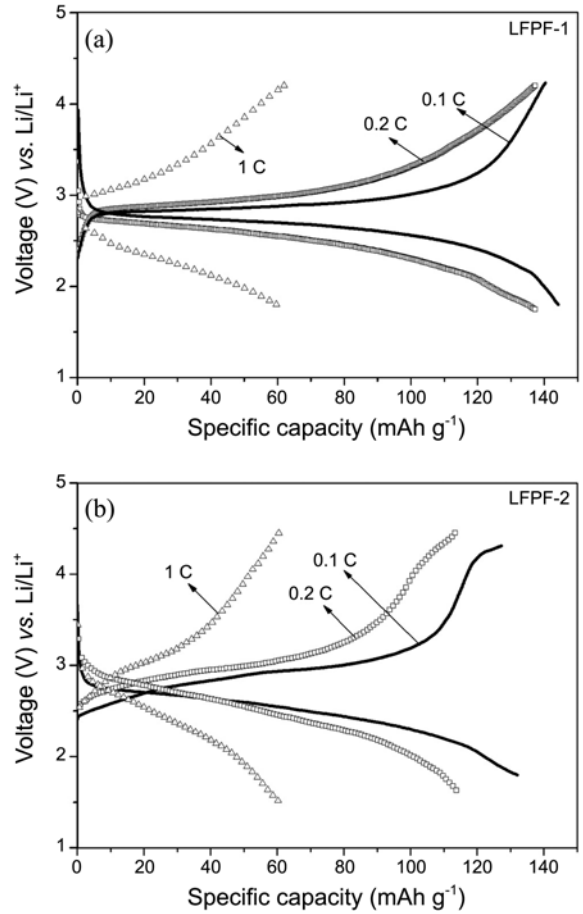

Figure 6. Discharge-charge curves at different rates of (a) LFPF-1 and (b) LFPF-2.

30 cycles, the capacity retention of LFPF-1 and LFPF-2 are 95.3% and 96.1%. The coulombic efficiency of the two samples are all above 97%, indicating the reversibility of the $LiFePO_4F$-Li_2FePO_4F transformation.

For the LFPF-1 and LFPF-2 samples, the galvanostatic discharge-charge performances at the different rates were studied. At 0.2 C, shown in Figure 6, LFPF-1 and LFPF-2 exhibit the capacity of 138 $mAh{\cdot}g^{-1}$ and 117 $mAh{\cdot}g^{-1}$ respectively and the plateaus become slight oblique result from polarization. With the elevation of the rate, the polarization increases obviously. At 1 C rate, the plateaus become shorter and more tilted, the capacity of the two samples are reduced to about 60 $mAh{\cdot}g^{-1}$, which were caused by poor electronic conductivity of the tavorite material reported by Recham *et al.* before.[2] Therefore, the charge compensation is unable to keep pace with the ionic transfer at a high rate, resulting in the decay of the capacity and the high polarization. However, the material for the testing cells is raw $LiFePO_4F$ without modification and the modifications for enhancing electronic conductivity are under exploration during the submitting of this manuscript.

Before the EIS tests, the half-cells were charged to 2.8 V. Figure 7(a) shows the Nyquist plots, each of them was composed of a semicircle in high frequency region and a tail

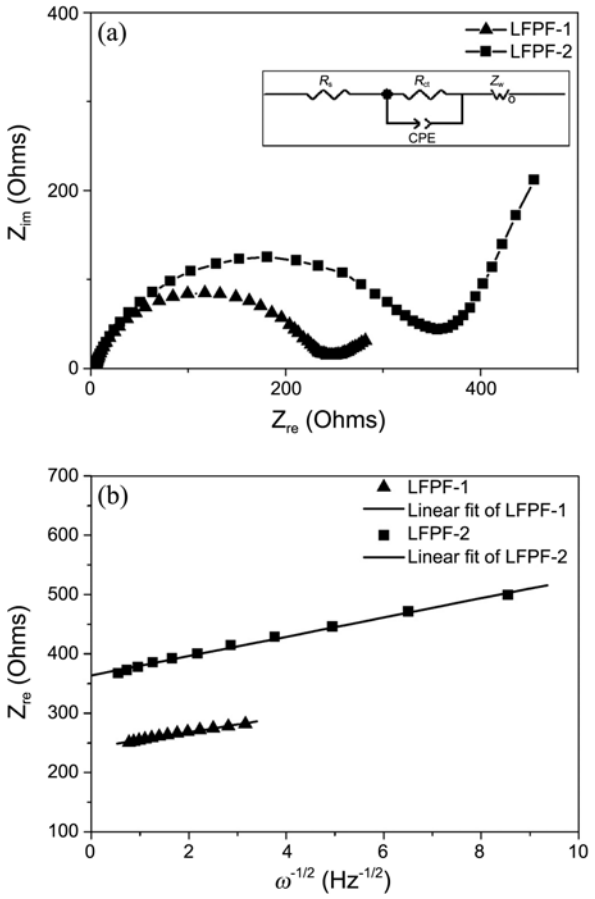

Figure 7. (a) Nyquist plots of the two samples at 2.8 V and the equivalent circuit (inset). (b) Zre-ω-1/2 plots derived from the low frequency tail of the Nyquist plots.

in low frequency one. The equivalent circuit is showed in the inset of Figure 7(a). The ohmic resistance (R_s) of the electrolyte and electrode is equal to the intercept at the Z_{re} axis. The charge transfer resistance (R_{ct}) is indicated by the radius of the semicircle in the middle frequency range. And the Warburg impedance (Z_w), represented by the low frequency tail, is associated with Li^+ diffusion in the material particles. A constant phase element CPE was placed to represent the double layer capacitance and passivation film capacitance. The R_{ct} of LFPF-1 and LFPF-2, which is related to complex reaction process of charge transfer between the electrolyte and the active materials,[11,12] are 240 Ω and 350 Ω, respectively. Therefore, the electrode composed of LFPF-1 exhibits a little more feasible Li^+ diffusion and electron transfer. Furthermore, the diffusion coefficients of Li^+ in LFPF-1 and LFPF-2 were calculated from EIS results.

The Li^+ diffusion coefficient is calculated according to the following equations[13]:

$$D = R^2T^2 \times (2A^2n^4F^4C^2\sigma^2)^{-1} \quad (1)$$

$$Z_{re} = R_s + R_{ct} + \sigma\omega^{-1/2} \quad (2)$$

Where in the Eq. (1), D is the diffusion coefficient of Li^+, R is the gas constant, T is the absolute temperature, A is the surface area of the cathode, n is the number of electrons per molecule during oxidization, F is the Faraday constant, C is the concentration of Li^+, and σ is the Warburg factor which is related with Z_{re}, shown in Eq. (2).

In our experiment, the electrodes are pressed on round aluminum foils with the diameter of 10 mm, so the value of A is 0.785 cm^2. On the basis of the structure analysis results, the calculated value of C_1 (the subscript 1 stands for LFPF-1, later under similar usage) is 1.928×10^{-2} $mol{\cdot}cm^{-3}$, and C_2 is 1.922×10^{-2} $mol{\cdot}cm^{-3}$. The σ_1 and σ_2 can be obtained from the Z_{re}-$\omega^{-1/2}$ plots, which are shown in Figure 7(b). From the linear fits of the dots, the derived value of σ_1 is 13.04, and σ_2 is 16.25. Therefore, from the Eqs. (1) and (2), we know that the value of D_1 is 9.09×10^{-13} $cm^2{\cdot}s^{-1}$, and D_2 is 5.89×10^{-13} $cm^2{\cdot}s^{-1}$. It can be seen that LFPF-1 has a little faster Li^+ migration than LFPF-2.

Conclusions

In summary this work has implemented a systemic comparison of microstructure and electrochemical properties between the $LiFePO_4F$ synthesized by sol-gel process and ceramic process. Based on XRD and SEM analysis, the samples synthesized by the two methods are both isostructural with the natural tavorite $LiFePO_4(OH,F)$, but the sol-gel route can produce smaller particles with a narrow size distribution. From the results of electrochemical characterizations we can see that the sample prepared by sol-gel process exhibit higher capacity, lower polarization and faster Li^+ migration than the sample prepared by conventional ceramic method. Therefore, the sol-gel synthesis is an effective way to improve the electrochemical properties of $LiFePO_4F$.

Acknowledgments. This work was financially supported by Chinese 863 program (No. 2008AA031205).

References

1. Ramesh, T. N.; Lee, K. T.; Ellis, B. L.; Nazar, L. F. *Electrochem. Solid-State Lett.* **2010**, *13*, A43.
2. Recham, N.; Chotard, J. N.; Dupont, L.; Delacourt, C.; Walker, W.; Armand, M.; Tarascon, J. M. *Nat. Mater*. **2009**, *9*, 68-74.
3. Barker, J.; Saidi, M. Y.; Swoyer, J. L. *J. Electrochem. Soc.* **2003**, *150*, A1394.
4. Barpanda, P.; Chotard, J. N.; Delacourt, C.; Reynaud, M.; Filinchuk, Y.; Armand, M.; Deschamps, M.; Tarascon, J. M. *Angew. Chem. Int. Ed.* **2011**, *50*, 2526.
5. Tripathi, R.; Ramesh, T. N.; Ellis, B. L.; Nazar, L. F. *Angew. Chem. Int. Ed.* **2010**, *49*, 8738.
6. Marx, N.; Croguennec, L.; Carlier, D.; Wattiaux, A.; Cras, F. L.; Suard, E.; Delmas, C. *Dalton T.* **2010**, *39*, 5108.
7. Reddy, M. V.; Subba, Rao, G. V.; Chowdari, B. V. R. *J. Power Sources* **2010**, *195*, 5768.
8. Qiao, X.; Yang, J.; Wang, Y.; Chen, Q.; Zhang, T.; Liu, L.; Wang, X. *J. Solid State Electrochem.* **2011**, DOI:10.1007/s10008-011-1512-7.
9. Recham, N.; Chotard, J. N.; Jumas, J. C.; Laffont, L.; Armand, M.; Tarascon, J. M. *Chem. Mater.* **2010**, *22*, 1142.
10. Barker, J.; Saidi, M.; Swoyer, J. *US Pat* **2002**, 6855462 B2.
11. Liu, J.; Jiang, R.; Wang, X.; Huang, T.; Yu, A. *J. Power Sources* **2009**, *194*, 536.
12. Molenda, J.; Ojczyk, W.; Marzec, J. *J. Power Sources* **2007**, *174*, 689.
13. Bard, A.; Faulkner, L. *Electrochemical Methods*; 2nd ed.; Wiley: New York, U. S. A., 2001; p 231.